Available online at www.sciencedirect.com

ScienceDirect

materialstoday: PROCEEDINGS

[ITME 2021]

# Correlating tool wear to intact carbon fibre contacts during drilling of Continuous Fibre Reinforced Polymers (CFRP)

John McClelland[a], Adrian Murphy[b], Yan Jin[b] and Saurav Goel[c,d,e*]

[a] *Northern Ireland Technology Centre, Queen's University Belfast, BT9 5AH, Northern Ireland.*
[b] *School of Mechanical and Aerospace Engineering, Queen's University Belfast, BT9 5AH, Northern Ireland.*
[c] *School of Engineering, London South Bank University, 103 Borough Road, London SE1 0AA, UK*
[d] *University of Petroleum and Energy Studies, Dehradun, 248007, India*
[e] *Indian Institute of Technology Guwahati, Guwahati, 781039, India*

**Corresponding author Email:* goels@lsbu.ac.uk

**Abstract**

Drilling holes to facilitate the mechanical joining of CFRP assemblies is a key operation for many high value products, especially in aerospace manufacturing. Tool wear continues to remain a significant operational problem and the extant research indicates that this wear initiates at the cutting edge due to the abrasive contact between the reinforcing fibres and the tool surface. While there have been efforts made to characterise and understand the wear process, the current literature lacks an explanation on the most logical influential parameters affecting it. Here, in this work, a novel method of calculating the idealised number of abrasive contacts between the reinforcing fibres of the workpiece and the tool is demonstrated. Sequentially, a systematic experimental study is designed to measure how tool wear is influenced by the calculated number of abrasive contacts and how wear shape varies, from an initial pristine cutting edge to a worn geometry. The experiments showed a consistent "waterfall" wear shape, the magnitude of which grew with the number of intact fibre-tool contacts. The study establishes that wear is focused on the flank face, while the junction with the rake face occurs at a repeatable radius in each experimental trial. The results also showed that the tool wear increases as a function of both drilled depth and drilling contact time, independent of drilling speed and feed, but notably, the wear magnitude does not scale proportionally with the number of idealised intact fibre-tool contacts.



*Keywords: CFRP, Drilling, Abrasion, Tool wear, Edge rounding, Thermal Imaging*

**Abbreviations:**

| | |
|---|---|
| 2D | Two Dimensional |
| 3D | Three Dimensional |
| CER | Cutting Edge Rounding |
| CES | Cutting Edge Segment |
| CFRP | Carbon Fibre Reinforced Polymers |
| CNC | Computer Numerically Controlled |
| Co | Cobalt |
| HMC | High Modulus Carbon |
| MAC | Multiplied Abrasive Contacts |
| NITC | Northern Ireland Technology Centre |
| NUC | Non-Uniformity Corrections |

| | |
|---|---|
| POI | Point of Interest |
| PVC | Polyvinyl Chloride |
| ROI | Region of Interest |
| VBA | Visual Basic for Applications |

**Nomenclatures:**

| | |
|---|---|
| $D_f$ | Fibre diameter |
| $d_{UC}$ | Unit cell length |
| $f$ | Feed rate |
| $l_{CES}$ | Cutting edge segment length |
| $M_z$ | Torque about global Z-axis |
| $n$ | Number of flutes |
| $T_g$ | Glass transition temperature |
| $V_c$ | Cutting speed |
| $V_f$ | Fibre volume fraction |
| $X_0$ | Global X-axis |
| $X_{CES}$ | Cutting edge segment X-axis |
| $X_{Total}$ *wear length* | Wear length parallel to X axis |
| $Y_0$ | Global Y-axis |
| $Y_{CES}$ | Cutting edge segment Y-axis |
| $Z_0$ | Global Z-axis |
| $Z_{CES}$ | Cutting edge segment Z-axis |
| $a_0$ | Depth of cut in global coordinate system |
| $a_{CES}$ | Depth of cut in cutting edge segment co-ordinate system |
| $\alpha$ | Flank face clearance angle |
| $\alpha_1$ | Point angle of cutting edge 1 |
| $\alpha_2$ | Point angle of cutting edge 2 |
| $\alpha_n$ | Point angle of cutting edge "n" |
| $\gamma$ | Rake face clearance angle |
| $\theta$ | Fibre angle |

## 1. Introduction

The drive for weight reduction and more efficient transport systems, without negating the strength and safety of the vehicle is at the forefront of current engineering research. Carbon Fibre Reinforced Polymers (CFRP) is a promising material when conducting this research. Wang et *al.* [1] and Butler-Smith et *al.* [2] state that CFRP is being used increasingly in transport products, due to their high specific stiffness and good corrosion resistance. Mechanical fastening of CFRP subcomponents requires the drilling of holes. Current practice and existing literature has largely focused on the quality of the hole and workpiece damage. Many advancements have been made to control both hole quality and workpiece damage such as fuzzing and push out delamination [3]. One of the great outcomes of such research has been that delamination free drilling of CFRP components is achievable, albeit a demanding task. However, only a select number of works are direct in studying tool wear during drilling of CFRP and most importantly on its prediction using an analytical approach.

Feito and Miguelez [4] and Park et *al.* [5] suggested that the tool wear during drilling of CFRP occurs through abrasion. Both Ahmad and Kalpakjian and Schmid [6,7] state how it has generally been assumed that hard particles in the workpiece, under high contact pressure, indent into the tool, creating micro grooves in the tool surface. Park et *al.* [5,8] surmised that such types of wear results from intact fibres, scraping on the surfaces of the tool as they are being cut. Torrance [9] stated that wear occurs due to hard abrasive particles (powder like chips from cut fibres) contacting the tool. Kumar and Singh [10] and Niu and Cheng [11] noted it to be due to the way chips are evacuated from the hole, while Merino-pérez et *al.* [12] found this can also occur if they have been embedded into the polymer matrix of the workpiece. Ahmad and Li [6,13] agree that diffusive or corrosive wear are not commonly found when drilling CFRP, as the required temperatures are not present. Nor has erosive wear been considered, due predominantly to the lack of coolant or lubricant typically used when drilling CFRP subcomponents for the purpose of assembly.

Faraz et *al.* and Ramirez et *al.* [14,15] disclose that the dominant form of abrasive tool wear is Cutting Edge Rounding (CER), in which wear is uniformly distributed along the length of the cutting edge. Thus, it is apparent that the traditional measurement of flank wear when machining metal, as documented in ISO 3685, 8688-1 and 8688-2 [16–18], has been interlinked to the measurement of CER when drilling CFRP. However, it is important to note, that quantifying either flank wear or CER does not automatically enable the quantification of the other.

It may be noted that the reinforcing carbon fibre constituent of CFRP composites is what makes the CFRP material abrasive and brittle. Therefore, it can be postulated that the frequency of the interactions between the fibres and the drill tool must remain an influential factor in governing the tool wear. Surprisingly, no works have attempted to quantify the relevant contribution of intact fibre abrasion wear, and if this is more important than fibre particle abrasion wear.

The objective of this study is to experimentally vary the number of intact carbon fibre contacts for a drilling process and capture the rate of tool wear and the shape of tool wear. It is envisaged that by varying the number of theoretical fibre contacts, by adjusting the drilling parameters, it may be possible to gain new insight into the relevant contribution of intact fibre abrasion wear. Accordingly, the subsequent sections of this paper present a short summary of the most relevant literature examining tool wear resulting from drilling CFRP. This is followed by detailing the experimental research methodology including details of the approach developed to analytically calculate the number of theoretical intact fibre contacts during a drilling process, before the novel data showing the correlation between the frequency of contact between fibres and the tool is discussed in light of the shape change of the tool.

## 2. Literature review

Having identified the importance of abrasive wear, this section reviews literature on abrasive wear contact mechanics and preceding tool wear CFRP drilling experimental studies, respectively. The section concludes with a summary of the specific knowledge gaps this paper identifies and work to be undertaken to address the research problem stated in the Introduction section

### *2.1. Abrasive wear contact mechanics*

Much work on abrasive wear, like that of Nathan and Jones and Pintaude et *al.* [19,20] assumes the materials to be homogeneous. In these works, the abrasive wear is microscopic cutting by an asperity of a different material. This form of abrasion requires the abrasive asperity to be at least 1.2 times harder than the material which is being abraded. Rabinowicz [21] states, if the hardness of the asperity is lower than this, then the rate of abrasion is dramatically reduced, but it is still present. Shaw and Dirke [22], alongside Archard and Hirst [23], identified relationships between the volume of material worn, the contact conditions and material properties of the abraded material. For the relationships to be accurate an empirical constant was required, which was found to vary with sliding speed, temperature and material. Childs et *al.* [24] developed the work of Archard and Hirst [23], producing an abrasive wear model for metals, the key difference being the replacement of the empirically derived coefficient with one based on the geometry of the abrasive asperity. However, without a calibrated empirical coefficient, the validation experiments showed the magnitude of wear was orders of magnitude less than those estimated from the model. Iliescu et *al.* [25] applied an extended version of Archard and Hirst's [23] model to the drilling of CFRP with tools of various coatings to estimate the tool wear. Various input parameters and coefficients were derived from a complex set of twenty-three experiments and a close correlation between the model and experiments was found with the use of calibrating coefficients. Most recently, Halila et *al.* [26,27] conducted research similar to Childs et *al.* [24]. During metallic turning operations, an arbitrary number of abrasive particles ($1x10^5$) was used to calculate the volume of wear removed from the tool. With the use of the selected number of abrasive particles, the model was found to closely match with the accompanying experiments. In all of these works, the abrading contacts are empirically captured within the calibrating coefficient. It is noteworthy that none of these works attempt to directly calculate the number of contacts, their locations or duration of contact with the tool.

Considering relatively 'soft' materials, such as CFRP, and how they wear 'hard' cutting tools, such as tungsten carbide, it is necessary to consider the individual constituent materials. Nathan and Jones [19] propose that the bulk hardness of the material being abraded is generated from the individual hardness' of the constituent materials and it is the softer constituents which are worn by the abrasive particles. This hypothesis of Nathan and Jones [19] was complimented in the work of Rawat and Attia [28]. In their study, they found that the abrasion of the tools when drilling CFRP could be separated into two similar modes; hard abrasion and soft abrasion. This categorisation

correlates with the individual hardness of the constituents which form the tool; the hard tungsten carbide (WC) grains and the relatively softer cobalt (Co) binder. Hard abrasion occurs when the repeated impacts from the workpiece fibres fracture the WC grains. Merino-pérez et *al.* [12] states that hard abrasion can be referred to as carbide grain polishing, subsequently followed by grain pull-out. Rawat and Attia [28] defined soft abrasion as damage of the Co binder (which has a lower hardness than the WC grains). It is best explained using the analogy of a brick, cemented into a wall. If the cement (representing the binder) is rapidly worn away, the brick (representing the WC grain) is no longer firmly held in place and can be easily removed as a whole. For example, Rawat and Attia [28] state that the repeated hard abrasion impacts could facilitate rapid crack nucleation in the Co binder surrounding the WC grain and thus the support offered by the cracked material (Co binder) to the WC grain will be decreased. Merino-pérez et *al.* [12], again studying CFRP drilling, found that the division of hard and soft abrasion was influenced by factors such as the cutting speed and the individual workpiece constituents and their combination. Interestingly, Merino-pérez et *al.* [12] extensive experimental results suggest that tool wear progresses faster by hard abrasion (polishing and subsequent grain pull-out) than by soft abrasion (binder removal).

Other research into abrasive wear mechanisms have considered the movement of the abrasive particle compared to the body that wears. Luo and Dornfeld [29], when studying solid-solid contact between an abrasive pad and wafer of material, separated abrasive particles into two categories; those acting by two-body abrasion and those acting by three-body abrasion. In their study, Luo and Dornfeld [29] found that almost all of the effective material removal occurred by two-body abrasion. Transferring this theory to a CFRP drilling operation, and considering the research reviewed thus far, it is logical to class any uncut fibres within the CFRP matrix, coming in contact with the cutting edges of the drill, as two-body abrasive particles. Likewise, fractured reinforcing fibre chips alongside fractured grains of cutting tool which are yet to be evacuated from the hole, can be classed as three-body abrasive particles. These classifications correlate with the results of Wang et *al.* [30] who stated any uncut carbon fibres protruding from the hole wall and any loose chips at the cutting zone, loose grains of WC, may abrade the flank face of the tool in a grinding motion. However, Wang et *al.* [30] failed to act further on this statement, choosing not to investigate how the number of uncut fibres protruding from the wall affected the rate or magnitude of tool wear.

### *2.2. Experimental studies*

It is now essential to review how experimental investigations into tool wear when drilling CFRP aligns with the previously summarised research. Firstly, Faraz et *al.* and Wang et *al.* [14,30] investigated the effect of varying tool geometries on wear rate. Likewise, Che et *al.* [31] built upon this to investigate the positive effect of providing coatings on the wear rate. Additionally, Ali et *al.* and Liu et *al.* [32,33] investigated the effect of process parameters on the rate of tool wear. Furthermore, the material constituents have been investigated in the works of Merino-pérez et *al.* [12,34]. In general, the experimental studies identify and quantify how process parameters influence a geometric measure of tool wear. Predominantly, these works focus on a single magnitude to describe tool wear, even if more complex three-dimensional imagery of the cutting edge is captured, as was completed by Merino-pérez et *al.* [12,34]. Importantly, these works do not routinely discuss or present information on the potential asperity contacts, their locations or durations with the tool. Thus, the shape of wear and potential contact data is not routinely captured, which impedes a coherent understanding on the tool wear mechanisms. Rather, at best, the experimental results of Merino-pérez et *al.* [12,34] appear to correlate with the noted theories of hard and soft abrasion as well as two-body and three-body abrasive wear, however the mechanisms of wear are not elucidated.

### *2.3. Summary and knowledge gap*

Abrasive wear models have been proposed by Archard and Hirst, Childs et *al*. and Iliescu et *al.* [23–25] containing both process and material parameters responsible for wear. However, the determination of parameters, particularly the number of abrasive wear contacts has not been addressed and is noted as an issue in preceding works of Halila et *al.* [26,27]. Existing experimental CFRP drilling tool wear investigations have, albeit, investigated the effect of changing process parameters (spindle speeds, feed rates, tool coatings, workpiece constituents) but lack a definitive explanation as to why this process change has adjusted the rate or magnitude of wear. Identifying this knowledge gap, this work will use an experimental approach to estimate in real-time the number of abrasive contacts between the reinforcing fibres and the tool as a function of process parameters and capture how the wear shape and its evolution is influenced by a change in the number of abrasive contacts between intact reinforcing fibres and the tool.

## 3. Methods

### *3.1. Materials, tooling and fixturing*

Gurit's Pre-impregnated HMC150 SE84LV was selected for the study as a workpiece material which has a high modulus carbon fibre and a hot-melt epoxy resin [35]. SE84LV is a low viscosity resin used in high stress structures. The high modulus carbon (HMC) reinforcing fibres of 7µm diameter give an overall mass of 150g/m$^2$ per ply, fibre volume fraction of 0.62 and ply thickness of 0.16mm. Detailed material properties are listed in Table 1. 68 plies of alternating direction, typical of a primary structure (load bearing structure) were laid-up on aluminium tooling plate (400mm × 272mm) before being cured at 120°C under one bar of vacuum for one hour. Figure 1 illustrates a cross section of the laminate during the curing process. The use of non-perforated release film and acrylic resin dams were specifically chosen to limit resin bleed to a minimum. No excess resin bleed was noted post process. Including the duration to ramp-up to temperature, dwell and ramp-down, the process took a total of four hours and twenty-seven minutes. Post cure, six individual test coupons of sizes 125mm × 125mm × 10.98mm were cut from a single laminate using a waterjet cutter. Four 12mm holes were drilled at the corner of each square coupon to fasten it to the drilling fixture plate.

Table 1 – CFRP workpiece material properties

| Properties | Value | Unit | Reference |
|---|---|---|---|
| Transverse modulus of fibre | 15 | GPa | [36] |
| Longitudinal modulus of fibre | 385 | GPa | [37] |
| Elastic modulus of resin matrix | 3.9 | GPa | [38] |
| Transverse modulus of resin matrix | 6.39 | GPa | [37] |
| Longitudinal modulus of resin matrix | 187.43 | GPa | [37] |
| In plane shear modulus | 4.31 | GPa | [37] |
| Fibre diameter | 7 | µm | [37] |
| Transvers Poisson's ratio of CFRP | 0.01 | | [37] |
| Longitudinal Poisson's ratio of CFRP | 0.337 | | [37] |
| Tensile strength of fibres | 4.9 | GPa | [38] |
| Matrix glass transition temperature (Tg) | 140 | °C | [39] |

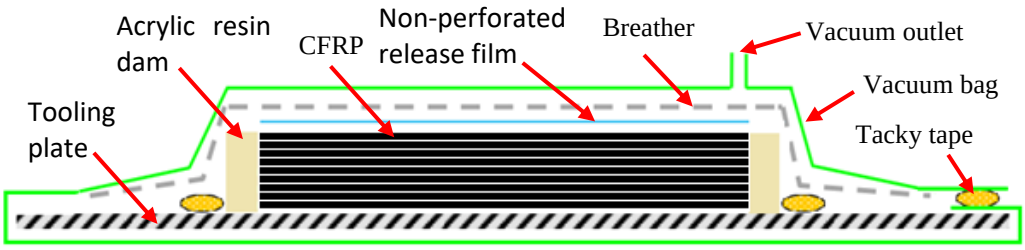


Fig 1. Architecture of vacuum stack when curing laminate

An uncoated tungsten carbide (WC) variant of SECO Tools' commercially available, double pointed, 6.38mm, SD205A-6.38-34-8R1-C1 drill, was chosen for the experiments. The special edition uncoated tool, which is identical to the commercially available coated version apart from being omitted from the coating process, was selected as the 'Baseline' tool, in an effort to ensure adequate tool wear was present. Detailed tool properties are listed in Table 2 while a schematic of the drill tool is shown in Figure 2. A Deckel FP3A 3-axis CNC drilling platform was chosen for its high speed spindle, $X_0$-$Z_0$ translating table and arrangement for chip extraction. Chip extraction was achieved

through a high flow Nerderman vacuum system with a 5µm HEPA filter. A custom designed and 3D printed extraction hood, encircled the tool and was held by a semi-rigid, positionable extraction hose at a height of 20mm above the drill tip. The wrap around design and positioning of the hood facilitated chip extraction without contaminating the force data (Figure 3).

Table 2 – Properties of the drill tool

| Property | Value | Unit |
|---|---|---|
| Manufacturer | SECO | - |
| Style | Twist drill | - |
| Base material | Tungsten carbide | - |
| Coating | N/A | - |
| Binder | Cobalt | - |
| Through tool coolant | Yes | - |
| Number of flutes | 2 | - |
| Diameter | 6.38 | mm |
| Shank diameter | 8 | mm |
| Point angle | 130 | ° |
| Secondary point angle | 60 | ° |
| Length | 5 x Diameter | mm |

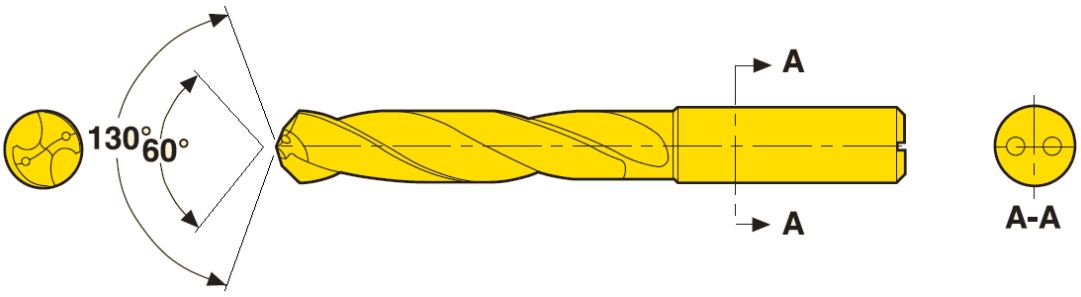


Fig 2. Schematic drawing of the drill tool

Within the 100mm diameter working area of each coupon, 80 holes were drilled in a staggered pattern while ensuring equispacing between each hole as shown in Figure 4 a). The drilling tool was programmed to move from left to right, then down to the next row, always beginning a new row at the left of the coupon. As the machine repositioned the tool above the first hole of a new row, it was noted that the extraction system remained in operation and this movement took more time than moving between subsequent holes in the same row. Additionally, due to the thermal properties of reinforcing fibres in an insulative polymer matrix, existing works by Fu et *al.* and Merino-Pérez et *al.* [40,41] have shown that temperatures in the local vicinity of a freshly drilled hole could exceed 150°C. Considering these points, it was expected that the thermal conditions at the commencement of each new hole may not remain uniform across all holes. A purpose-built CNC programme was used to ensure that the tool tip and CFRP coupon would both remain at ambient temperature when initiating the first hole of each batch of ten (this is shown later on in Figure 7). The drilled holes separated by 1.5 times the hole diameter (Figure 4 b) showed consistent interply bonding strength of the bottom-most plies and prevented premature push out delamination. The hole exit condition were observed to worsen due to the tool wear initially shown as uncut carbon fibres (Figure 4 b) and resulting in spalling and sub-surface delamination (Figure 8).

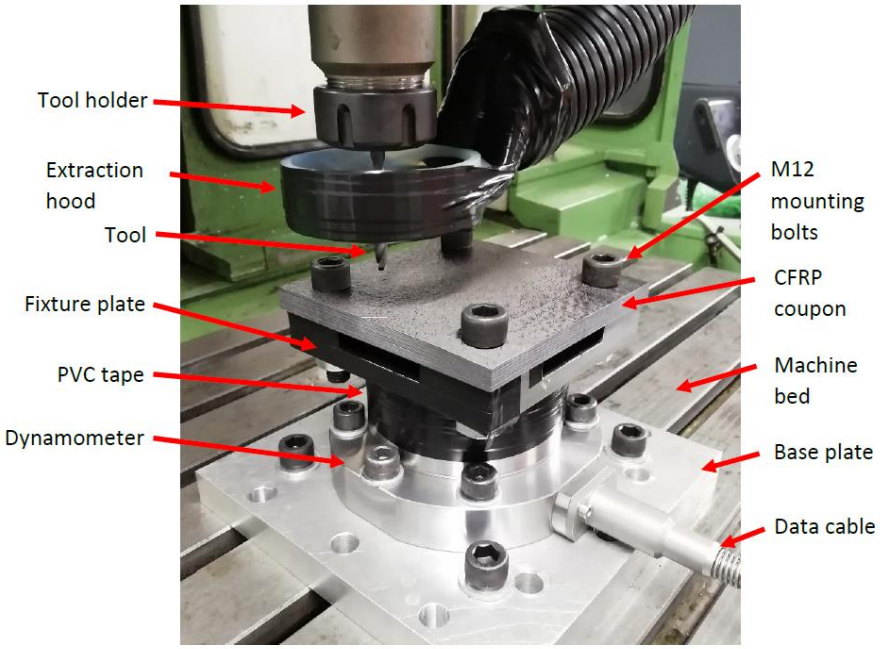


Fig 3. Experimental set-up

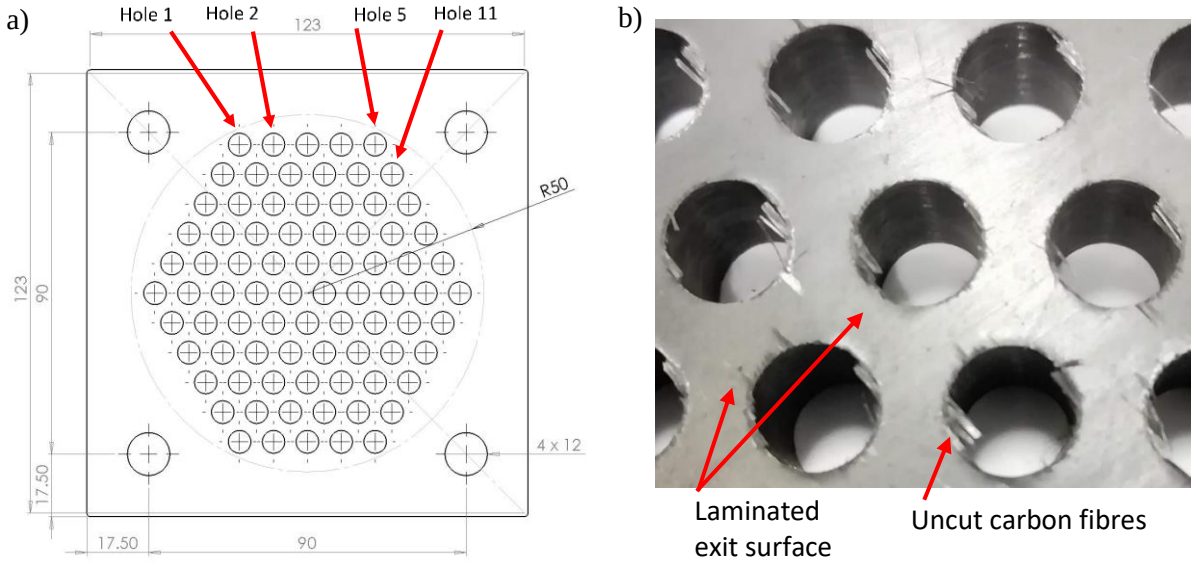


Fig 4. (a) Coupon schematic and drilling pattern (dimensions in mm) (b) exit surface of CFRP coupon (experiment 1)

### *3.2. Measurement apparatus*

A Kistler four component piezoelectric dynamometer, type 5070 multi-channel amplifier and Kistler's Dynoware Type 2528D-02 software were used to record the forces in the $X_0$, $Y_0$ and $Z_0$ directions (see Figure 9 a)), as well as the torque about the $Z_0$ axis (Mz).

The temperature of the tip of the tool when exiting the CFRP was measured using a FLIR A6751SC thermal imaging camera and ResearchIR thermal imaging software. The use of this equipment is much less time consuming

yet closely comparable with that of embedded thermocouples [12]. Positioned to the side of the machining bed on a tripod, the camera lens was collinear with the X-axis of the test coupon (see figure 9 a)). Visible at the tool tip is a circular region of interest (ROI) which was used to take an average value of temperature for the multiple pixels (and hence data points) within its boundaries (Figure 5). Prior to drilling, the emissivity of a tool was calculated at elevated temperatures, using PVC tape of known emissivity as a control, as recommended by camera manufacturers. The reflected environmental light within the field-of-view was measured prior to any drilling trials and this information was input to the FLIR software. Furthermore, the same camera shroud, backing plate, safety enclosure and workshop lighting were used across all drilling processes. Lastly, any reflective surfaces of the dynamometer and fixture plate within the field of view were coated with PVC tape of known emissivity. Prior to recording, manual Non-Uniformity Corrections (NUC) were completed as per manufacturer's instructions, ensuring the camera maintained its accuracy (>100°C ±2% of reading (±1% typical) [42]). Due to the machine bed controlling the movements in the $X_0$ direction, the tool tip remained in close focus during drilling at all times.

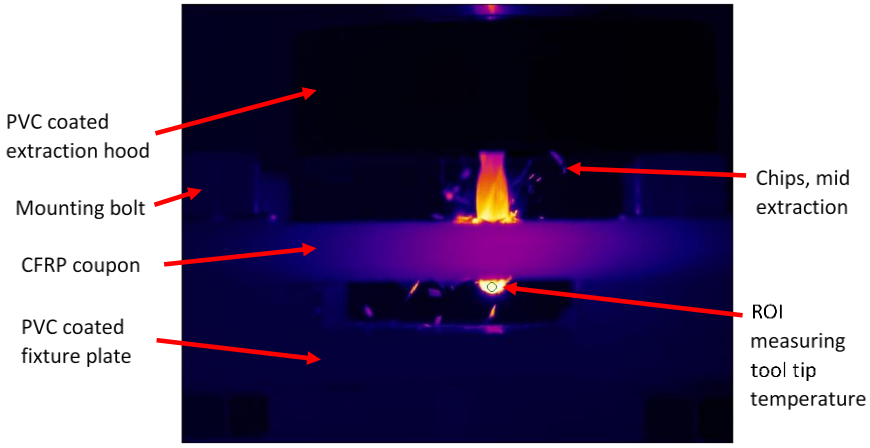


Fig. 5. Field of view from thermal imaging camera mid drilling. The hottest regions emit the brightest light.

An Alicona InfiniteFocus G5 Optical microscope in conjunction with an unique custom made tool holding apparatus [43] were used for on-machine measurement of the tool wear. Constructed from aluminium alloy and Stratasys VeroBlue 3D printing polymer, the tool holding apparatus facilitated the repeatable positioning of the tool and tool holder under the lens within 100µm. Once positioned, a customised MultiEdge measurement routine within Alicona's EdgeMaster software module was programmed to facilitate the automated measurement of the chisel, primary and secondary edges of the tool (Figure 6). A vertex between the relief face and through tool coolant hole, was used as a reference point for final alignment before the automated measurement programme was executed. Throughout all experiments, the same Point Of Interest (POI) on the secondary cutting edge, at a height of 2.50mm above the chisel point and a radius of 3.09mm from the axis of tool rotation was chosen for detailed inspection (Figure 6).

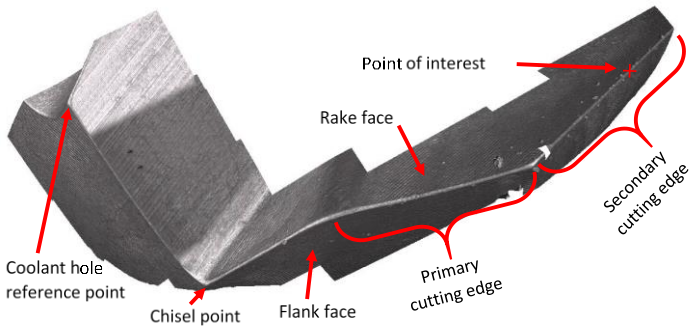


Fig. 6. 3D view of tool tip from Alicona microscope

*3.3. Drilling procedure*

Drilling was made in batches of ten holes, as illustrated by the experimental flowchart (Figure 7). Due to the vast amount of memory required when recording data across the appropriate temperature range, only before and after the final hole of each batch was the tool tip temperature recorded. Theoretically, the drilling of the final hole was expected to coincide with the largest tool temperature during each batch of ten holes. At the end of the tenth hole, the CNC programme was paused, the tool holder was removed from the machine and the tool was cleaned using compressed air and degreasing wipes with a soft touch. The tool was subsequently placed on the Alicona microscope and the coolant hole reference point was aligned in the Alicona software. During the tool wear measurement process, the CFRP coupon was visually inspected for signs of excessive pull-up or push out delamination. If any delamination width in the preceding ten holes exceeded 40% of the hole diameter, the tool was deemed to be worn and the experiment was ended (Figure 8). The delamination boundary value is critical for the structural integrity of the final assembled product and is typically defined through combined mechanical analysis and physical testing. If delamination was acceptable, the drilling process was cleared to move on to the next iteration of ten holes (Figure 7).

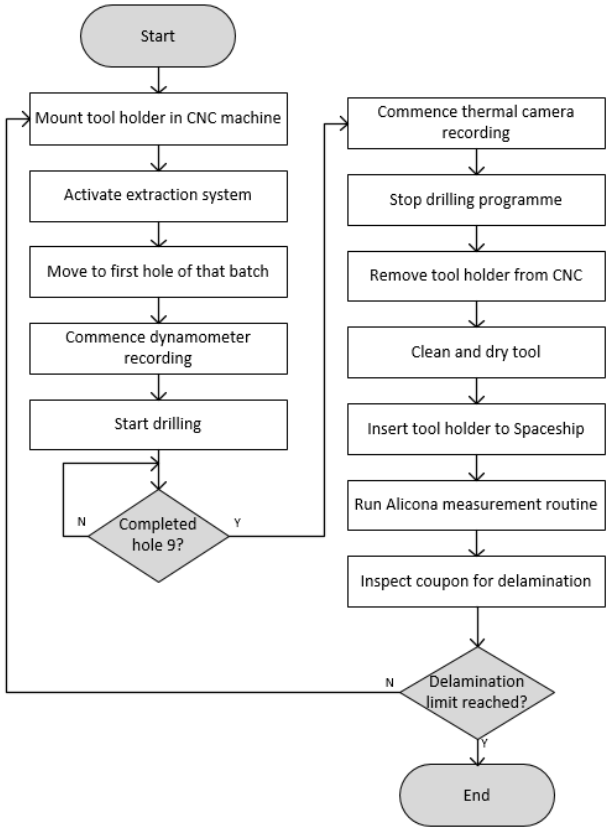


Fig. 7. Drilling process and method of data acquisition

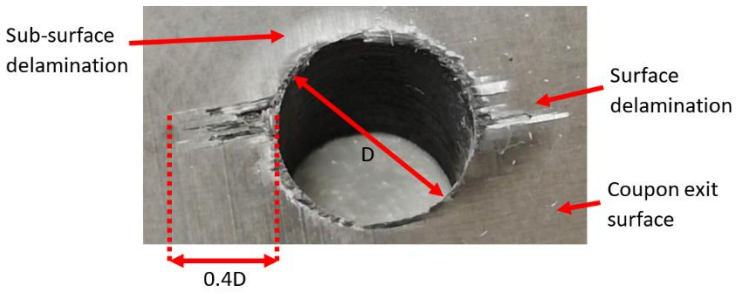


Fig. 8. Excessive push-out delamination

### *3.4. Design of experiments*

The investigation consisted of three individual experiments as detailed in Table 3. The first experiment ('Baseline') used drilling speeds and feeds recommended by the tooling manufacturer. The second experiment was a direct 'Repeat' of the 'Baseline'. The third experiment investigated the effect of increasing the number of abrasive tool wear contacts by increasing the cutting speed and reducing the feed rate. The cutting speed used in the 'Multiplied Abrasive Contacts' ('MAC') test case is double that employed in the 'Baseline' test case, yet still within the manufacturers recommended speed range. Likewise, the reduction in the feed rate does not force the tool to operate in unsafe conditions. As shown in the final column of Table 3, the number of abrasive contacts per hole more than quadrupled for the last experiment. The methodology used to calculate the number of abrasive contacts per hole, based on the process parameters (Table 3), is presented next.

Table 3 – Design of experiments

| Experiment number | Experiment Test Case | Cutting speed (m/min) | Feed rate (mm/min) | Number of abrasive contacts per hole ($x10^3$) |
|---|---|---|---|---|
| 1 | Baseline | 75.0 | 187.1 | 333.6 |
| 2 | Repeat | 75.0 | 187.1 | 333.6 |
| 3 | Multiplied Abrasive Contacts (MAC) | 150.0 | 112.3 | 1370.2 |

### *3.5. Methodology to calculate the number of theoretical intact fibre contacts*

To quantify the number of abrasive contacts between the reinforcing fibres and the tool, the path of the cutting edge Point of interest (POI) must be modelled. Along the path, it is also essential to capture the workpiece properties, in particular the fibre orientation with respect to the cutting edge POI orientation. To this end, a co-ordinate system is required. Figure 9 a) shows a tool resting on a CFRP workpiece. The co-ordinate system overlaid to this diagram is fixed to the workpiece, with the $X_0$-$Y_0$ plane parallel with the workpiece and the $Z_0$ axis collinear with the axis of rotation of the tool. Similar to preceding works [44–46], the workpiece constituents may be represented as cylindrical fibres, equally spaced throughout the homogeneous resin matrix. As illustrated in Figure 9 b), taking a magnified cross-sectional view of a single CFRP ply, a fibre is centrally located within a circle of resin matrix. The length of a unit cell ($d_{uc}$) may thus be calculated using equation (1) where $D_f$ represents fibre diameter and $V_f$ represent fibre volume fraction. Note that a single ply within a laminate will be several unit cells thick

$$d_{UC} = \sqrt{\frac{\pi\left(\frac{D_f}{2}\right)^2}{V_f}} \tag{1}$$

Next, the tool must be discretised. Firstly, an element from the cutting edge is defined as a Cutting Edge Segment (CES). The size of this portion is directly related to the geometry of the tool and the length of a unit cell $d_{UC}$, and

may be calculated using equation (2). Taking any arbitrary point along the length of a cutting edge of a drill, the CES relating to that point would be constructed as illustrated in Figure 9 c). Angle $\alpha_n$ from Figure 9 c) represents the angle of the cutting edge upon which the arbitrary point is located, where subscript $n$ is an integer, representing the cutting edge in question. For example, a double-edged twist drill would have point angles of $\alpha_1$=120° and $\alpha_2$=140° for the primary and secondary cutting edges, respectively. In the knowledge that drills rarely have straight cutting edges, a straight line-of-best-fit, inclined at half the cutting edge angle ($\alpha_n$) can be drawn, with the arbitrary POI being coincident with the mid-point. This line would be of length $l_{CES}$, as defined in Figure 9 c). From here, the construction of two planes, one at each end of the line $l_{CES}$ and perpendicular to the line $l_{CES}$ become the boundaries to the CES, as shown in Figure 9 c).

$$l_{CES} = \frac{d_{uc}}{\cos\left(\frac{\alpha_n}{2}\right)} \tag{2}$$

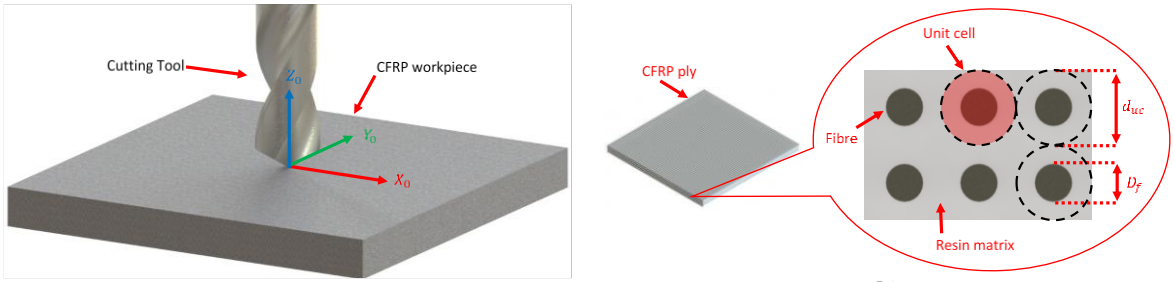


**a)** **b)**

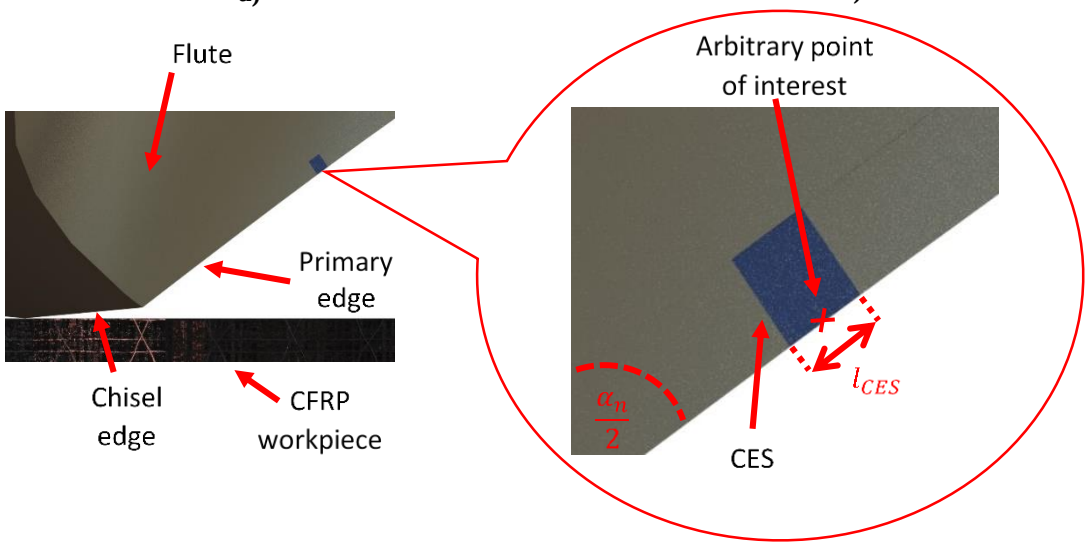


**c)**

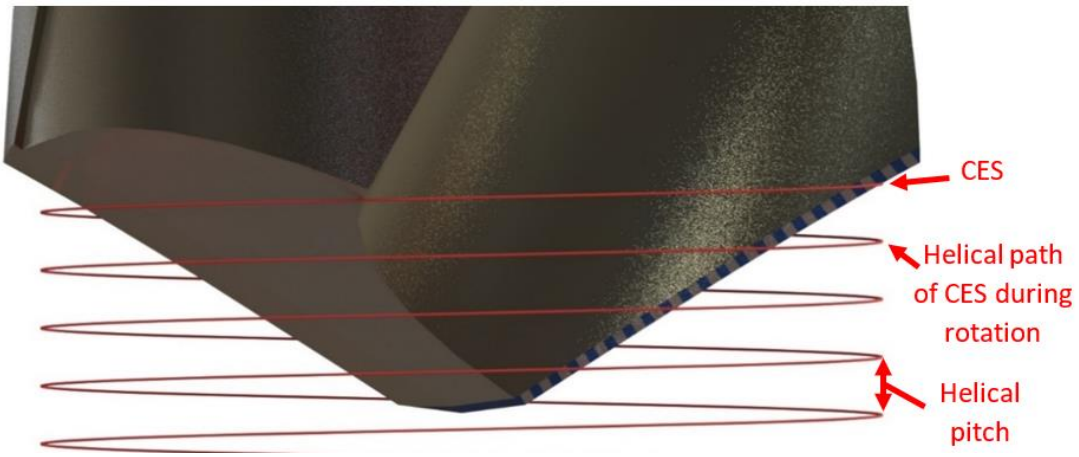


**d)**

Fig 9. Tool and work-piece idealisation – part 1.

Returning to a lower magnification of the tool tip, viewed from the $X_0$-$Z_0$ plane of the global co-ordinate system, the theory behind the depth of cut for the tool may be clarified. Focusing on the labelled CES within Figure 9 d), as the tool rotates, the CES would follow a helical path as denoted by the line in the figure. For every complete rotation of the tool, the CES would have translated down by a distance equal to the pitch of the helix. However, due to the number of cutting edges on the tool, a calculation using equation (3) is required to determine the true depth of cut $a_0$ per cutting edge. In equation (3), $f$ is the feed rate (m/min), $V_c$ is the cutting speed (rev/min) and $n$ is the number of cutting zones (the number of flutes on a twist drill).

$$a_0 = \frac{f}{nV_c} \tag{3}$$

$$a_{CES} = \frac{a_0}{\cot\left(\frac{\alpha_n}{2}\right)} \tag{4}$$

Next we consider the workpiece, by assuming an idealised scenario where the drilling process is instantaneously stopped. The bottom surface of the hole will be of a conical form and the ends of numerous fibres would be coincident with this surface. A 3D rendering of such an idealised condition for an arbitrary point in time is shown in Figure 10 a). For clarity in this image, the majority of the tool has been omitted, leaving only a few neighbouring CES in situ. From this image, it can be recognised that a cutting edge will become engaged and successively disengaged with the exposed ends of the fibres, as it rotates about its axis. A single arbitrary fibre, just ahead of the cutting edge, is highlighted in Figure 10 a). For this single arbitrary fibre, a plane may be constructed. This plane is coincident with the central axis of the fibre and normal to the axis of rotation of the tool, Figure 10 b) and Figure 10 c). In these figures the clearance angles for the rake and flank faces are denoted by $\gamma$ and α respectively. The contact angle that the fibre makes with the cutting direction (measured clockwise) is $\theta$. At this stage, it is necessary to introduce a second co-ordinate system specifically for the purposes of describing the fibre-tool, abrasive contacts within this plane of tool and workpiece material (the CES co-ordinate system). The $Y_{CES}$ axis is parallel and opposite to the instantaneous cutting direction, while the $X_{CES}$ axis points radially outwards, into the uncut CFRP. The $Z_{CES}$ axis (not shown in the figure) is parallel with and in the same direction as the $Z_0$ axis (Figure 9 a)).

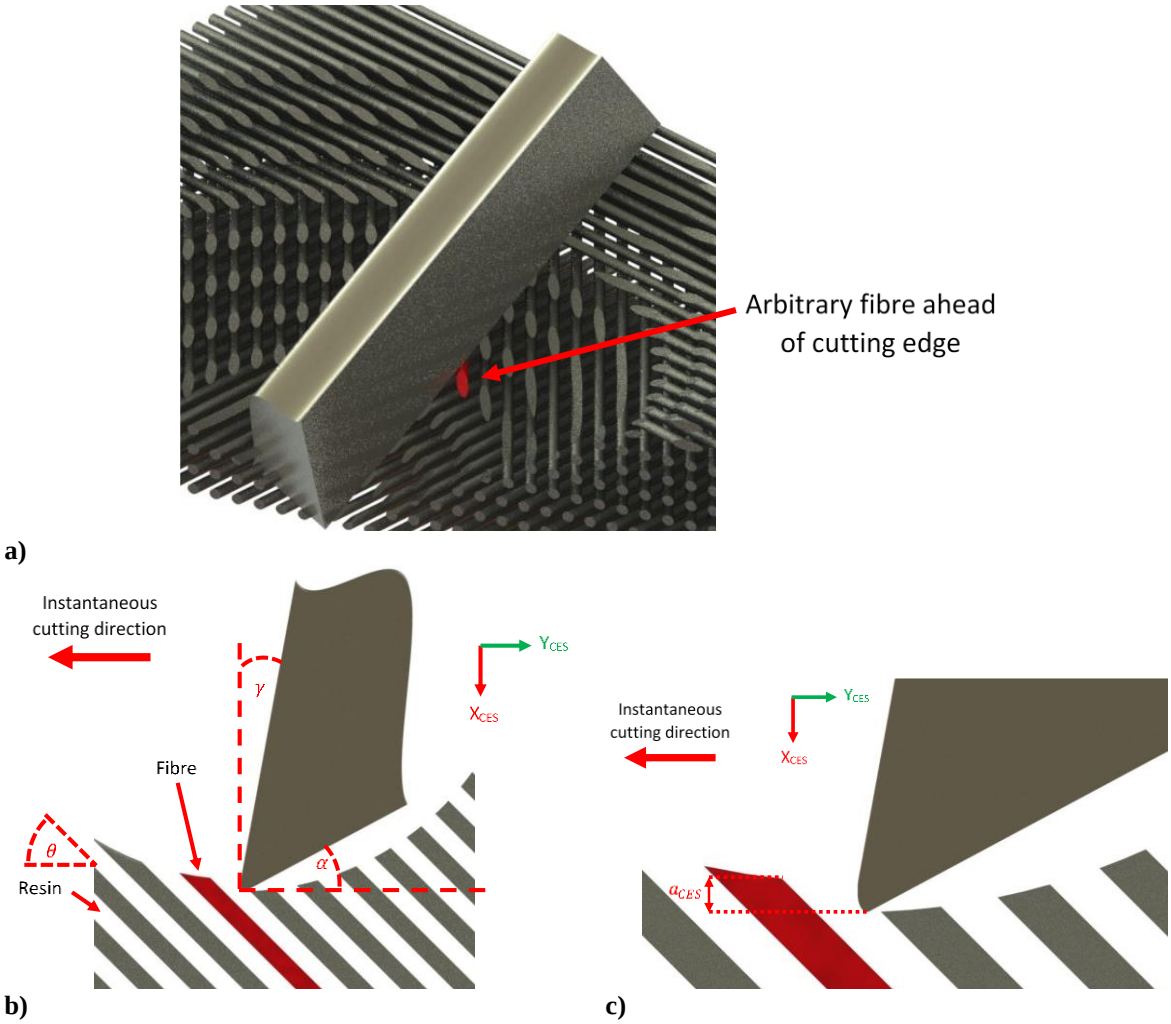


Figure 10 – Tool and work-piece idealisation – part 2.

Any changes in the depth of cut $a_0$ as derived in Figure 9 d) and equation (3), will influence the depth of cut when viewing a fibre-tool abrasive, contact through the 2D discretisation method illustrated in Figure 10 b). Taking a magnified view of the cutting edge (Figure 10 c)) we can create a new parameter for the depth of cut in the CES co-ordinate system. Using trigonometric identities for complementary angles, equation (4) can be produced, where $\alpha_n$ is the point angle for the cutting edge in question. The methodology used here to discretise the tool down to a 2D version could be applied to any fibre, with respect to any point along the multiple CES that make up the complete cutting geometry of the tool. In each case, the complete list of potential variables is limited to $\gamma$, $\alpha$ and $\theta$.

Finally, it is not possible to idealise the initial contact orientation between the POI and the upper surface of the workpiece. When a rotating tool is brought down into contact with a workpiece, the true start point of the first arc of rotation, could be anywhere within a full 360° rotation of the $X_0$ axis. Therefore, it is only possible to examine different initial contact orientations and assess how these influence the number of fibre POI contacts and the local orientation between the POI and the fibre at these contacts. Thus, the above calculations were encoded into a Microsoft Excel workbook using VBA scripts, as outlined in Figure 11. The encoded method was then used to predict, for the 'Baseline' experiment defined in Table 3, the POI rotating through its cutting path and to calculate the number of contacts and the local orientation between the POI and the fibre at contact. Calculations were performed considering a series of initial points of contact between the POI and the upper surface of the workpiece. Starting with an initial contact where the tool $X_0$-$Y_0$ axis aligned with the top ply local material axis, and then in 15° increments for a total of 360°. From all twenty-four start points of the first arc of rotation, and for the baseline drilling parameters (Table 3),

the mean number of abrasive contacts for a complete hole was calculated as $341.8\times10^3$ while the largest deviation from the mean by any individual start point was found to be 0.11%. Thus, the degree of rotation of the tool's POI on first contact with the workpiece was deemed to have a negligible effect on the total number of contacts. Furthermore, dividing the contacts into three groupings based on the relative orientation between the POI and the fibre (1 to 90°, 91 to179°, 0° or 180°; see fibre angle $\theta$ of Figure 10 b)) the number of contacts in each grouping also do not significantly vary with the first contact assumed.

Although the calculations have assumed a 'perfect' workpiece with equal spacing and perfect fibre alignment and the cutting process has been assumed not to locally change the fibre geometry (from local cutting damage and deformation), the approach provides a method to predict the number and orientation of contacts. Such calculations will be appropriate to classify the experiment if the tolerances in spacing and alignment are equivalent for each specimen. This is believed to be the case herein as each coupon is manufactured from the same batch of materials and using the same process, tools and operators. Therefore, the method will be used in the following experimental section when defining each of the experimental arrangements and discussing experimental wear results.

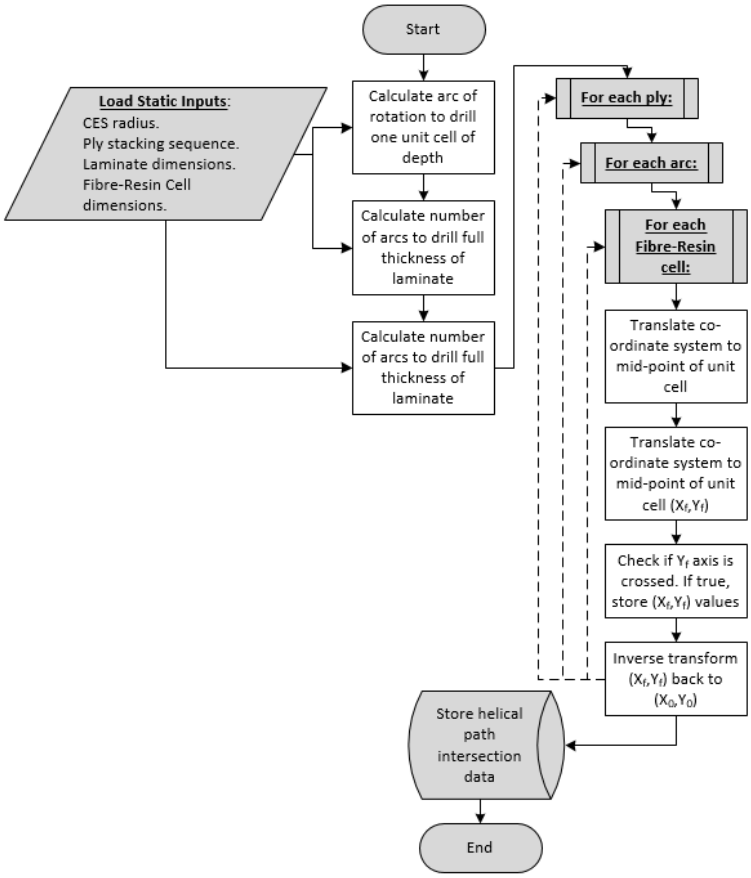


Fig. 11. Method of calculating contacts between cutting edge point of interest and workpiece fibres

## 4. Results

Throughout the presented results, with reference to the 'MAC' test case, the data for the holes 1 to 31 and 111 to 120 was lost due to computer corruption and hence neglected.

### *4.1. Forces and torque measurements*

Figure 12 shows the thrust forces during drilling for all three experiments. Considering the 'Baseline' experiment first, the thrust force was found to increase non-linearly with the number of drilled holes. This finding in itself

corresponds with the majority of literature already published on this subject and is emotive of wearing of the tool's cutting edges, as documented by Merino-pérez et *al.* [12]. However, this does not inform us directly about either the magnitude or the form of tool wear. It is notable also that the thrust force fluctuates with every five to eight holes. This is also visible for the other experiments. This was also alluded to by Merino-pérez et *al.* [12] where the drilling pattern influences the length of time the tool is separated from the workpiece. Considering the drilling pattern in Figure 4 a), it can be verified that each fluctuation in the thrust force of Figure 12 corresponds to one of two things. The tool has either had a lengthened cutting dwell as the CNC table moved from the last hole of the previous row (right of coupon) to the first hole of the next row (left of coupon) or lengthened dwell between the 10th hole of one data set and the first hole of the subsequent set (see Figure 7 for reference). In either case, both the tool tip and workpiece material in the local vicinity of the hole will have different thermal conditions than the previous hole, both cooling during the intervening period.

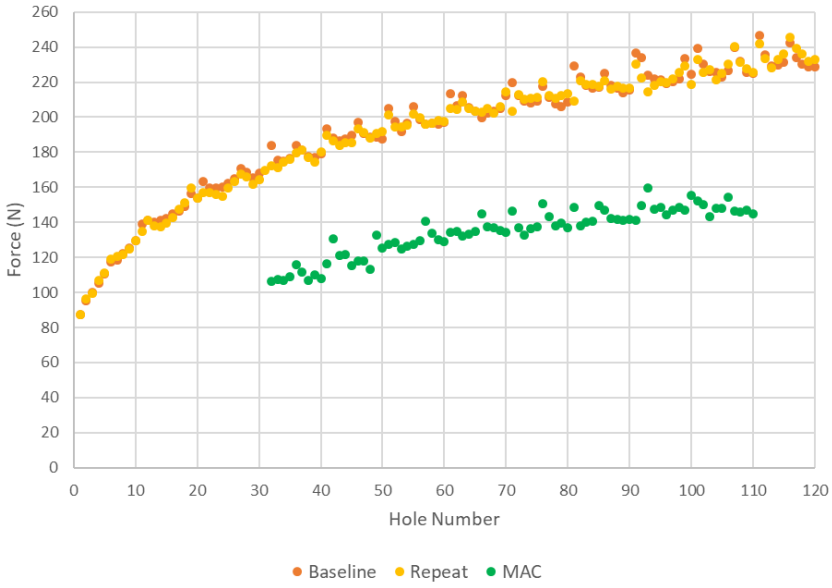


Fig 12. Thrust force ($Z_0$-axis) for all experiments

Considering the torque about the $Z_0$ axis (Mz), it is much more difficult to find any informative pattern within the recorded results. The average torque about the $Z_0$ axis (Mz) across all 'Baseline' holes was recorded as 0.32Nm however, the spread of recorded values spans from a minimum value of 0.14Nm to a maximum of 0.51Nm across the 120 holes of the 'Baseline' case. As such, the torque variation across the life of the tool is deemed much less significant than the thrust force variation shown in Figure 12.
Reviewing the 120 holes of the 'Baseline' experiment in Figure 12, a 178% increase was recorded, where the measured force increases rapidly for the first 30 holes before slowing and reaching a more stable rate of increase. The same trend was obtained for the 'Repeat' experiment. Considering the 'MAC' experiment the increase in thrust forces was seen to be similar in trend but slower to that of the 'Baseline' experiment. The noticeable reduction in thrust force compared to the 'Baseline' experiment is most likely caused by the reduced feed rate. It is not possible to infer from these force results directly, the form or magnitude of wear in each experiment.

### *4.2. Wear profiles*

Tool wear occurred by abrasive mechanisms with no evidence from visual inspection of the tool surfaces of erosive, diffusive, adhesive, corrosive or fracture mechanisms. Figure 13 illustrates the measured wear profiles for each of the three cases. For each experiment, the profiles are rotated such that the Y-axis is parallel to the tangential, instantaneous cutting direction. This was completed in two stages. Firstly, an automated Microsoft Excel VBA script was used to

globally align and superimpose each worn profile onto the original sharp profile. This alignment occurred at a large distance from the cutting edge (≈600µm) for both the rake and flank faces. Secondly, a groove on the rake face approximately 50µm above the original cutting edge, formed during tool manufacture (see Figure 6 for reference) and common across all profiles was used for final manual alignment of the profiles. The rake face and flank face are labelled within the 'Baseline' test case (see Figure 6 for reference).

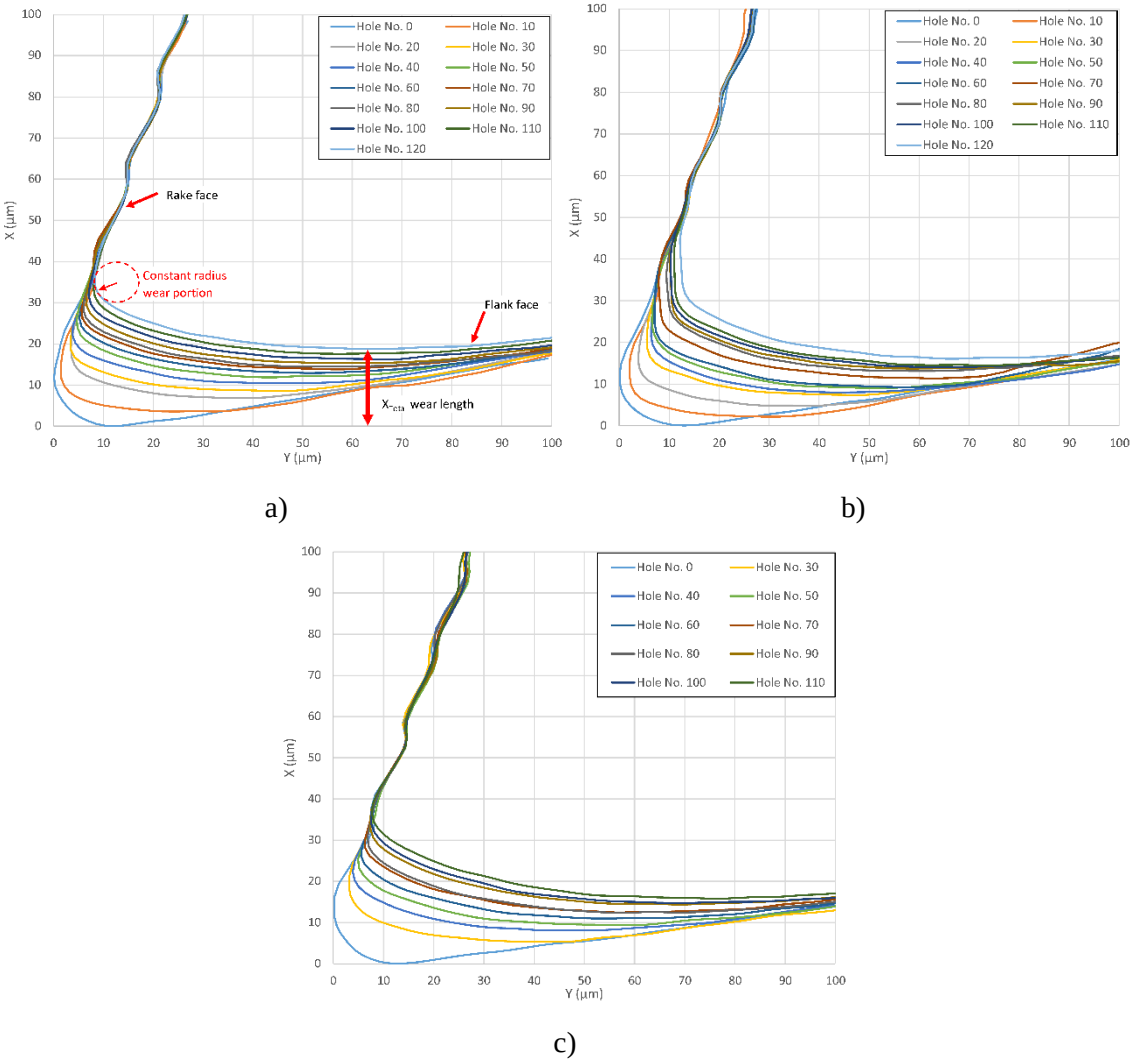


Fig. 13. Tool wear profiles for (a) Baseline (b) Repeat (c) MAC experiments

All tools exhibit significant edge rounding wear. The majority of tool wear occurs as a rounding of the nose, particularly at the connection to the flank face, while a constant radius is identified where the rake face transitions into the cutting edge. Both Wyen et *al.* [47] and the microscope manufacture, [48] describe these wear profiles as "waterfall" wear profiles and it is clear that these profiles are consistent across all experiments, irrespective of the number of holes drilled. Thus, the shape of tool wear is consistent irrespective of the number of abrasive contacts between the reinforcing fibres and the tool and independent of the drilling parameters.

Having identified the common wear profile shape for each experiment, it is possible to consider a parameter to describe and compare the magnitude of wear. Acknowledging Astakhov's [49] point that there is no accepted edge round wear measurement technique, a generic method of quantifying wear magnitude was employed. For each iteration of 10 holes, the linear distance, parallel to the X-axis, between the original, sharp tool geometry and the point of inflection of the worn rounded edge, was measured. This $X_{Total}$ *wear length* parameter is illustrated for the 120th

hole of the 'Baseline' experiment in Figure 13 a). For comparison purposes it may be interesting to consider multiple locations in the X and Y orientation however herein only one is illustrated for brevity. Using a single magnitude measure, it becomes possible to plot the progression of wear during the drilling of the 120 holes. Figure 14 a) and b) plot, for each experiment in Table 3, the exemplar wear parameter ($X_{Total}$ $wear\ length$) on the vertical axis. This is plotted against, on the horizontal axis, the total drilled depth in Figure 14 a) and total drilled time in Figure 14 b), which are common variables used in the literature when considering wear magnitude properties. A third, new variable – the number of theoretical intact carbon fibre contacts, is plotted against the wear magnitude in Figure 14 c), where the number of contacts is calculated using the method outlined in Section 3.4.

Considering first the plot of wear magnitude versus drilled depth, Figure 14 a), it is clear that the change in process parameters (speed and feed rates) do not significantly influence the rate of 'wear magnitude versus drilled depth'. Considering the plots of wear magnitude versus contact time, Figure 14 b), there may be a common relationship across all experiments. Although, not as clear or conclusive as seen with drilled depth, there appears beyond the initial phase of high wear (>300mm, > 100 seconds) a similar rate of 'wear magnitude versus drilled time' for the three experiments.

Examining now the novel plot of wear magnitude versus the number of theoretical intact carbon fibre contacts, Figure 14 c), the rate of wear magnitude is different for each experiment. This is particularly noteworthy when considering each experiment demonstrated similar gradients when plotted against drilled depth and contact time. There are clear differences in the wear rates per number of theoretical intact carbon fibre contacts. It is clear that there is not a single proportional relationship, beyond the initial phase (>300mm, > 100 seconds), between the number of intact fibre contacts and the wear magnitude. Having calculated the number of contacts it is possible to classify each contact as either acute or obtuse and plot these separately in the figure. This has only been done for the 'MAC' results in Figure 14 c). However, with a symmetric problem this simply reduces the magnitude of contacts by a factor of two, with both the acute and obtuse contacts equal in magnitude. It is interesting to note that only considering the acute (or obtuse) does reduce the difference in slope between the experiments. However, a significant offset remains between the baseline and MAC results.

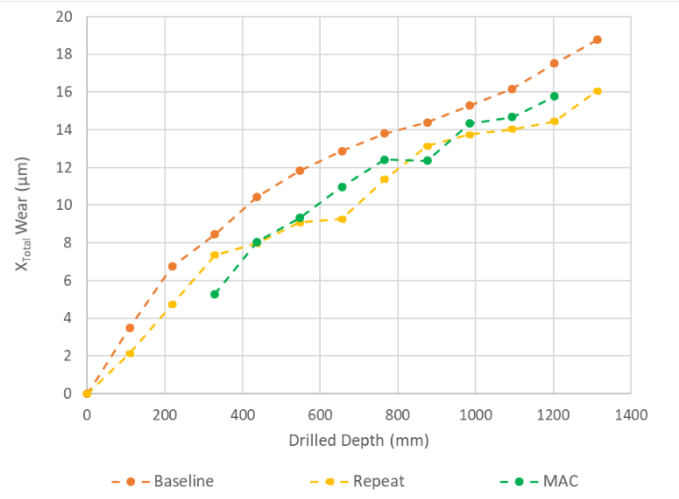


a)

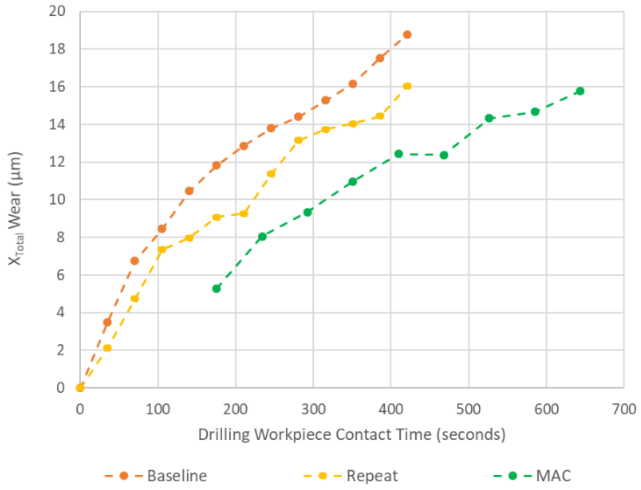


b)

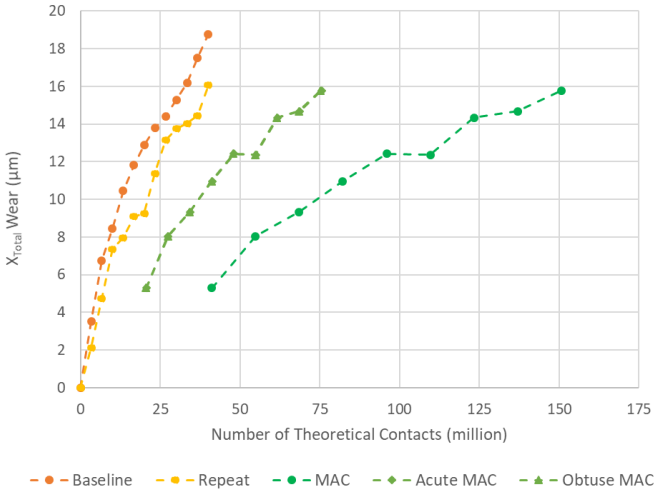


c)

Fig. 14. $X_{Total}$ *wear lengths* versus a) drilled depth, b) contact time and c) number of theoretical contacts. Note that the Acute and Obtuse MAC data points are identical.

### *4.3. Drill tip temperature*

For each experiment, there was no significant rise or fall in tool tip temperature as the number of drilled holes increased. As such, Table 4 shows the average tool tip temperature and standard deviation for each experiment. On average, the tool tip temperature of the 'MAC' experiment was 31°C higher than the 'Baseline' or 'Repeat' experiments. This equates to a 14.6% increase. These findings correspond with logic, in which the cutting speed and feed rate determine the length of time the tool is in contact with the workpiece as well as the thrust pressure. Thus, modifying the drilling parameters modifies the magnitude of heat built up by friction. In this respect, the number of abrasive tool wear contacts, the length of time the tool is cutting, and the global thrust force have impacted the heat generation when drilling. Significantly, in all experiments, the recorded temperatures of the tool tip irrespective of hole number, exceed the workpiece's resin glass transition temperature ($T_g$=140°C).

Table 4 – Tool tip temperature

| Experiment number | Experiment Test Case | Average Tool Tip Temperature (°C) | Standard Deviation |
|---|---|---|---|
| 1 | Baseline | 213 | 6.5 |
| 2 | Repeat | 213 | 7.9 |
| 3 | Multiplied Abrasive Contacts (MAC) | 245 | 10.5 |

## 5. Discussions on results

The unique wear rates between experiments seen in Figure 14 c) and the similar wear rates seen in Figure 14 a) (and somewhat similar wear rates seen in Figure 14 b)) indicate that by only considering the number of contacts the physical conditions which produce wear are not being fully captured. Returning to the theory outlined in Section 2.1, the models described in the literature include both the number or duration of asperity contacts along with the normal force between the asperity and the material being worn. Therefore, given the similar wear magnitude against drilled depth seen in Figure 14 a) the normal force between the contacting asperities and the tool is changing with the change in process parameters along with the number of contacts. These results together suggest that the number of intact fibre contacts only partly describes the mechanism for wear. A significant characteristic not captured here is the pressure between the tool and fibres, considering the idea that the fibres under contact pressure indent into the tool to form micro grooves. Although the local pressure at the cutting edge is not experimentally easily measurable, it is evident from Figure 12 that there is a different total force between the tool and the workpiece in the 'MAC' experiment. However, it is also necessary to point out that in addition to the change in total thrust force there is a change in drill tip temperature witnessed with the change in drilling parameters (but all above the glass transition temperature of the workpiece composite resin material). Finally, it is also important to reflect on the calculation method used to predict the number of contacts. This introduced several idealisations to the workpiece, in particular that the fibres are evenly distributed and perfectly aligned in each ply. Although this is a simplification each experimental setup is treated in the same way and the calculations may be expected to produce a consistent and appropriate number of contacts for comparison between the different experimental conditions.

It is interesting to note that when plotting wear magnitude versus drilled depth and contact time, there does appear to be a clear common relationship, independent of process parameters, for any experiment. The plotting of wear magnitude versus the number of intact fibre contacts does not appear to offer such a normalising effect when drilling parameters are changed. It is potentially necessary to consider the number of contacts along with the contact pressure or force in order to create a process parameter independent relationship with wear magnitude. On the other hand, although the measures of drilled depth and contact time appear to be good indicators describing the total 'window' in which particle contact and intact fibre contact wear is possible, neither time or depth directly describe the physical mechanics of an intact fibre or fibre particle being indented under pressure into the tool to scribe out a micro groove.

## 6. Conclusions

This paper has experimentally investigated the evolution of the shape and magnitude of cutting-edge rounding wear when drilling CFRP, in particular the effect of varying the number of abrasive contacts between the reinforcing fibres and the tool. From the experiments, the following conclusions can be drawn:

- The literature does not clarify as to how the number of fibre–tool interactions influences CFRP drilling tool wear, and if the number of intact carbon fibre contacts can be used as a reliable predictive parameter of wear by itself. This study, for the first time, demonstrates experimentally, that the wear magnitude does not scale proportionally with the number of idealised intact fibre-tool contacts.
- The shape of tool wear was consistent across all experiments, irrespective of the number of abrasive contacts between the reinforcing fibres and the tool. Most of the wear occurred at the junction of the cutting edge and the flank face, resulting in a sweeping "waterfall" shaped rounding of the cutting edge.
- The magnitude of wear, measured normal to the instantaneous cutting direction of the tool profile, appears to have a common relationship, independent of process parameters, with drilled depth and drilling contact time beyond an initial period where higher wear is seen. There is no common relationship, independent of process parameters, between the magnitude of wear, measured normal to the instantaneous cutting direction of the tool

profile, and the number of theoretical intact fibre contacts. The thrust force data was seen to be more sensitive to the in-process wear of the cutting edge in comparison to the torque data.

- Further research is required to assess the conditions in which a fibre must find itself to be capable of causing tool abrasive wear, and on phenomenological measures which capture the key wear mechanics. Focus should be placed on the effect of thermal softening of the workpiece and the properties associated with the tool's resistance to deformation when contacted by an abrasive fibre or fibre particle.

**Acknowledgements**

The support and funding from the Northern Ireland Technology Centre (NITC) of the Queen's University of Belfast is acknowledged. All authors greatly acknowledge the financial support provided by the UKRI via Grants No. EP/S036180/1 and EP/T024607/1, TFIN+ Feasibility study award to LSBU (EP/V026402/1), the Royal Academy of Engineering via Grants No. IAPP18-19\295 and TSP1332 and the Newton Fellowship award from the Royal Society (NIF\R1\191571). This work made use of Isambard Bristol, UK supercomputing service accessed by a Resource Allocation Panel (RAP) grant as well as ARCHER resources (Project e648).

**References**

[1] Wang X, Kwon PY, Sturtevant C, Kim DDW, Lantrip J. Comparative tool wear study based on drilling experiments on CFRP/Ti stack and its individual layers. Wear 2014;317:265–76. https://doi.org/10.1016/j.wear.2014.05.007.

[2] Butler-Smith PW, Axinte DA, Daine M, Kennedy AR, Harper LT, Bucourt JF, et al. A study of an improved cutting mechanism of composite materials using novel design of diamond micro-core drills. Int J Mach Tools Manuf 2015;88:175–83. https://doi.org/10.1016/j.ijmachtools.2014.10.002.

[3] Zhang HJ, Chen WY, Chen DC, Zhang LC. Assessment of the Exit Defects in Carbon Fibre-Reinforced Plastic Plates Caused by Drilling. Key Eng Mater 2001;196:43–52. https://doi.org/10.4028/www.scientific.net/KEM.196.43.

[4] Feito N, Miguelez MH. Numerical analysis of the influence of tool wear and special cutting geometry when drilling woven CFRPs. Compos Struct 2015;138:285–94. https://doi.org/10.1016/j.compstruct.2015.11.065.

[5] Park K-H, Beal A, (Dae-Wook) Kim D, Kwon P, Lantrip J. A Comparative Study of Carbide Tools in Drilling of CFRP and CFRP-Ti Stacks. J Manuf Sci Eng 2014;136:014501. https://doi.org/10.1115/1.4025008.

[6] Ahmad J. Machining of Polymer Composites. Boston, MA: Springer US; 2009. https://doi.org/10.1007/978-0-387-68619-6.

[7] Kalpakjian S, Schmid S. Manufacturing Engineering and Technology. Seventh. New Jersey: Pearson; 2013.

[8] Park K-H, Beal A, Kim D (Dae-W, Kwon P, Lantrip J. Tool wear in drilling of composite/titanium stacks using carbide and polycrystalline diamond tools. Wear 2011;271:2826–35. https://doi.org/10.1016/j.wear.2011.05.038.

[9] Torrance AA. Modelling abrasive wear. Wear 2005;258:281–93. https://doi.org/10.1016/j.wear.2004.09.065.

[10] Kumar D, Singh KK. An approach towards damage free machining of CFRP and GFRP composite material: a review. Adv Compos Mater 2014;3046:1–15. https://doi.org/10.1080/09243046.2014.928966.

[11] Niu Z, Cheng K. Multiscale Multiphysics-Based Modeling and Analysis on the Tool Wear in Micro Drilling Metal Matrix Composites (MMC). J Multiscale Model 2016;07:1640002. https://doi.org/10.1142/S1756973716400023.

[12] Merino-pérez JL, Hodzic A, Ayvar-soberanis S, Merson E. The Effect of Resin on Tool Wear in Machining CFRP - (PhD Thesis). University of Sheffield, 2016.

[13] Li B. A review of tool wear estimation using theoretical analysis and numerical simulation technologies. Int J Refract Met Hard Mater 2012;35:143–51. https://doi.org/10.1016/j.ijrmhm.2012.05.006.

[14] Faraz A, Biermann D, Weinert K. Cutting edge rounding: An innovative tool wear criterion in drilling CFRP composite laminates. Int J Mach Tools Manuf 2009;49:1185–96. https://doi.org/10.1016/j.ijmachtools.2009.08.002.

[15] Ramirez C, Poulachon G, Rossi F, M'Saoubi R. Tool wear monitoring and hole surface quality during CFRP drilling. Procedia CIRP 2014;13:163–8. https://doi.org/10.1016/j.procir.2014.04.028.

[16] International Organization for Standardization (ISO). ISO 3685 Tool life testing with single-point turning

tools. 1993.
[17] International Organization for Standardization (ISO). ISO 8688-1 Tool life testing in milling - Part 1:Face milling. 1989.
[18] International Organization for Standardization (ISO). ISO 8688-2 Tool life testing in milling - Part 2: End milling. 1989.
[19] Nathan GK, Jones WJD. Influence of the hardness of abrasives on the abrasive wear of metals. Arch Proc Inst Mech Eng Conf Proc 1964-1970 (Vols 178-184), Var Titles Label Vol A to S 1966;181:215–21. https://doi.org/10.1243/PIME_CONF_1966_181_317_02.
[20] Pintaude G, Bernardes FG, Santos MM, Sinatora A, Albertin E. Mild and severe wear of steels and cast irons in sliding abrasion. Wear 2009;267:19–25. https://doi.org/10.1016/j.wear.2008.12.099.
[21] Rabinowicz E. Friction and Wear of Materials. 2nd ed. New York: John Wiley & Sons; 1995.
[22] Shaw MC, Dirke SO. On the Wear of Cutting Tools. Int Inst Prod Eng Res - Microtec 1956;10:187–93.
[23] Archard JF, Hirst W. The Wear of Metals under Unlubricated Conditions. Proc Roy Soc L 1956;A236:397–410. https://doi.org/10.1098/rspa.1956.0144.
[24] Childs T, Maekawa K, Obikawa T, Yamane Y. Metal machining–theory and applications, 2000. London: Arnold; 2000.
[25] Iliescu D, Gehin D, Gutierrez ME, Girot F. Modeling and tool wear in drilling of CFRP. Int J Mach Tools Manuf 2010;50:204–13. https://doi.org/10.1016/j.ijmachtools.2009.10.004.
[26] Halila F, Czarnota C, Nouari M. New stochastic wear law to predict the abrasive flank wear and tool life in machining process. Proc Inst Mech Eng Part J J Eng Tribol 2014;228:1243–51. https://doi.org/10.1177/1350650114521405.
[27] Halila F, Czarnota C, Nouari M. Analytical stochastic modeling and experimental investigation on abrasive wear when turning difficult to cut materials. Wear 2013;302:1145–57. https://doi.org/10.1016/j.wear.2012.12.055.
[28] Rawat S, Attia H. Wear mechanisms and tool life management of WC-Co drills during dry high speed drilling of woven carbon fibre composites. Wear 2009;267:1022–30. https://doi.org/10.1016/j.wear.2009.01.031.
[29] Luo J, Dornfeld D a. Material removal mechanism in chemical mechanical polishing: theory and modeling. IEEE Trans Semicond Manuf 2001;14:112–33. https://doi.org/10.1109/66.920723.
[30] Wang F, Qian B, Jia Z, Fu R, Cheng D. Secondary cutting edge wear of one-shot drill bit in drilling CFRP and its impact on hole quality. Compos Struct 2017;178:341–52. https://doi.org/10.1016/j.compstruct.2017.04.024.
[31] Che D, Saxena I, Han P, Guo P, Ehmann KF. Machining of Carbon Fiber Reinforced Plastics/Polymers: A Literature Review. J Manuf Sci Eng 2014;136:034001. https://doi.org/10.1115/1.4026526.
[32] Liu D, Tang Y, Cong WL. A review of mechanical drilling for composite laminates. Compos Struct 2012;94:1265–79. https://doi.org/10.1016/j.compstruct.2011.11.024.
[33] Ali M, Xiang L, Yue D, Liu G. Assessment of Cutting Performance of Cemented Tungsten Carbide Drills in Drilling Multidirectional T700 CFRP Plate. J Manuf Mater Process 2018;2:43. https://doi.org/10.3390/jmmp2030043.
[34] Merino-pérez JL, Coromant S, Ab S, Park AM, Way M. The applicability of Taylor ' s model to the drilling of CFRP using uncoated WC-Co tools : the influence of cutting speed on tool wear. Int J Mach Mach Mater 2014;16:95–112. https://doi.org/10.1504/IJMMM.2014.064683.
[35] Gurit Holding. GURIT PRODUCT CATALOGUE - Europe, Middle East and Africa 2020;33:68.
[36] Arteiro A, Catalanotti G, Melro AR, Linde P, Camanho PP. Micro-mechanical analysis of the effect of ply thickness on the transverse compressive strength of polymer composites. Compos Part A Appl Sci Manuf 2015;79:127–37. https://doi.org/10.1016/j.compositesa.2015.09.015.
[37] Gurit. Mechanical Properties SE84LV HMC300 & HMC200.pdf. 2018.
[38] Gurit Holding. SE 84LV Low Temperature Cure Epoxy Prepreg General Datasheet. 2012.
[39] Gurit Holding. Product Processing Guide Epoxy Prepreg Processing. 2012.
[40] Merino-Pérez JL, Royer R, Ayvar-Soberanis S, Merson E, Hodzic A. On the temperatures developed in CFRP drilling using uncoated wc-co tools part I: Workpiece constituents, cutting speed and heat dissipation. Compos Struct 2015;123:161–8. https://doi.org/10.1016/j.compstruct.2014.12.033.
[41] Fu R, Jia Z, Wang F, Jin Y, Sun D, Yang L, et al. Drill-exit temperature characteristics in drilling of UD and MD CFRP composites based on infrared thermography. Int J Mach Tools Manuf 2018;135:24–37. https://doi.org/10.1016/j.ijmachtools.2018.08.002.
[42] FLIR Systems. FLIR A6750 SLS Longwave Infrared Thermal Camera | FLIR Systems 2017.

https://www.flir.co.uk/products/a6750-sls/?model=29439-251 (accessed December 9, 2020).
[43] Kelly J, Murphy A. Measuring Tool Wear When Drilling CFRP - (MEng Thesis). Queen's University Belfast: 2018.
[44] Xu J, Mkaddem A, El Mansori M. Recent advances in drilling hybrid FRP/Ti composite: A state-of-the-art review. Compos Struct 2016;135:316–38. https://doi.org/10.1016/j.compstruct.2015.09.028.
[45] Xu W, Zhang LC. On the mechanics and material removal mechanisms of vibration-assisted cutting of unidirectional fibre-reinforced polymer composites. Int J Mach Tools Manuf 2014;80–81:1–10. https://doi.org/10.1016/j.ijmachtools.2014.02.004.
[46] Chen L, Zhang K, Cheng H, Qi Z, Meng Q. A cutting force predicting model in orthogonal machining of unidirectional CFRP for entire range of fiber orientation. Int J Adv Manuf Technol 2017;89:833–46. https://doi.org/10.1007/s00170-016-9059-5.
[47] Wyen CF, Knapp W, Wegener K. A new method for the characterisation of rounded cutting edges. Int J Adv Manuf Technol 2012;59:899–914. https://doi.org/10.1007/s00170-011-3555-4.
[48] Bruker Alicona. Product Information - Edge Measurement Package 2017:1–19.
[49] Astakhov VP. The assessment of cutting tool wear. Int J Mach Tools Manuf 2004;44:637–47. https://doi.org/10.1016/j.ijmachtools.2003.11.006.